$^{57}Co(n,\gamma)^{58}Co$ reaction cross section: Thermal and resonance integral measurements and energy dependence

Nora L. Maidana,* Joel Mesa, Vito R. Vanin, and Ruy M. Castro
Laboratório do Acelerador Linear, Instituto de Física, Universidade de São Paulo, Travessa R 187, Cidade Universitária, CEP: 05508-900 São Paulo, SP, Brazil

Mauro S. Dias and Marina F. Koskinas
Laboratório de Metrologia Nuclear, Instituto de Pesquisas Energéticas e Nucleares. IPEN-CNEN/SP Travessa R 400, Cidade Universitária, CEP: 05508-900 São Paulo, SP, Brazil
(Received 17 March 2004; published 7 July 2004)

The $^{57}Co(n,\gamma)^{58}Co$ thermal and resonance integral cross section were measured as 51(5) b and 20.0(19) b, respectively, by irradiating aliquots of ^{57}Co solution sealed inside quartz bottles near the core of the IEA-R1 IPEN research reactor and counting the gamma-ray residual activity. The irradiations were monitored using Au-Al alloy foils, with and without Cd cover. The gamma-ray measurements were performed with a shielded HPGe detector. Westcott formalism was applied for the average neutron flux determination. The cross section energy dependence was evaluated using the multilevel Breit-Wigner expression considering the first two resonances and the statistical model for energies above the second resonance. Maxwellian averaged neutron capture cross section with neutron temperatures between 5 and 100 keV were also evaluated.

DOI: 10.1103/PhysRevC.70.014602 PACS number(s): 28.20.Fc, 25.40.Ny, 26.20.+f, 27.40.+z

I. INTRODUCTION

Neutron capture by light and intermediate mass nuclei is an important process in nuclear reactors, nucleosynthesis processes, and in the nuclear transmutation of fission product nuclides. Nevertheless, the thermal neutron capture cross section of a specific nuclide cannot be predicted by theoretical calculations. For energies near the first neutron absorption resonance, the separation between bound states embedded in the continuum is of the order of 1 keV, and the thermal cross section can be sensitive to changes of a few eV in the position of the first resonance. The currently available nuclear models cannot predict neither which will be the first level above the neutron separation energy nor the position of a level with such precision. An analogous comment can be made on the resonance integral cross section, which is defined as the nuclide average cross section in a $1/E$ neutron energy spectrum, because the resonances in the first few keV represent the major part of its value. Therefore the thermal and resonance integral cross sections can be assessed only by experimental methods. After these quantities were measured, nuclear model calculations can predict at least partially the cross-section energy dependence.

In recent years, the accurate knowledge of neutron capture cross sections of radioactive nuclei has become the focus of special attention in calculations related to spent fuel and accelerator driven nuclear energy systems, justifying the experimental effort to complete the already extensive database on neutron reaction cross sections. Since a theoretical framework for data evaluation is required to build any reliable database, it is important to explain the observed values in terms of nuclear parameters.

This paper reports the measurement of the thermal cross section and resonance integral of the reaction $^{57}Co(n,\gamma)^{58}Co$. To the best of our knowledge, this is the first measurement of these cross sections; a brief report was presented in the 2001 Conference on Nuclear Data for Science and Technology [1]. Besides being a relatively common radioisotope, ^{57}Co was found in SN 1987A supernova [2], calling attention to the possible nuclear processes involving this nuclide.

The experimental procedure was similar to that used in previous measurements of the $^{137}Cs(n,\gamma)^{138}Cs$ and $^{241}Am(n,\gamma)^{242}Am$ reaction cross sections [3,4]. We also determined the detailed energy dependence of the neutron absorption cross section using standard nuclear models. The obtained values differ considerably from those available in existing databases [5] that, however, were not based on experimental measurements, meaning that the discrepancy is not disclosing any special difficulty neither with the theoretical reaction model nor with the database evaluation criteria.

II. EXPERIMENTAL METHOD

The experiment consisted in the observation of the gamma-ray residual activity of the reaction product after irradiation in the reactor, where the main difficulty arose from the small target mass. Since the target is radioactive, increasing the target mass would preclude observation of the product residual radioactivity. Hence we had to find the proper balance between the different ensuing gamma-ray activities.

A. Decay schemes and observed radiations

Figure 1 shows the ^{57}Co and its neutron capture products radioactive decay schemes. The ^{57}Co decays by electron capture and gamma ray emission with a half-life of 271.70(9) d;

*Electronic address: nmaidana@if.usp.br

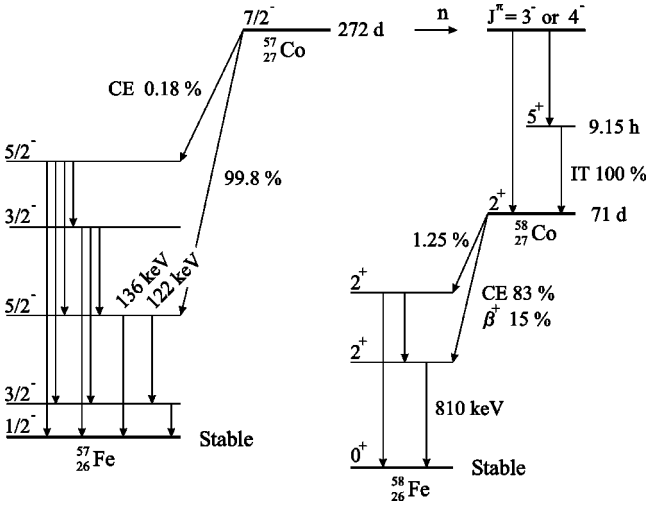

FIG. 1. ^{57}Co$(n,\gamma)^{58}$Co reaction and decay schemes [6].

the emission probabilities of the principal gamma-ray transitions, with energies 122.0614(3) keV and 136.4743(5) keV, are 85.60(17)% and 10.68(8)% per decay, respectively [6]. Following a neutron capture, the residual ^{58}Co nucleus can be found either in its metastable or ground state: the first one, with a half-life of 9.15(10) h, decays to the ground state mainly through internal conversion, and the second one, with a half-life of 70.82(3) d, decays by electron capture and β^+, followed by gamma-ray emission. The 810.775(9) keV gamma ray with 99.448(8)% emission probability [6] was used to determine the reaction product activity.

B. Target preparation

The ^{57}Co was obtained from an Amersham carrier-free solution. It was chosen an one-year-old production lot to reduce the activities of the contaminants ^{58}Co and ^{56}Co, with half-lives smaller than ^{57}Co. The ^{58}Co activity was used for calibration purposes as detailed in Sec. II D. This solution was diluted with HCl 0.1 M before utilization.

The samples to be irradiated were made from aliquots of ^{57}Co ($\sim$0.8 MBq) solution dropped inside quartz bottles with an external diameter of 9-mm and 1-mm wall thickness. The bottles with the ^{57}Co solution were placed inside a dryer, which was a recipient with silicon dioxide. After the solution had absolutely dried, the bottles were sealed to avoid external contamination or ^{57}Co activity loss.

C. Sample irradiation and average neutron flux determination

The irradiations were performed at the IPEN 5 MW pool-type research reactor operating at 2 MW. The samples were placed inside a sealed aluminum rabbit and irradiated near the reactor core, in the EIRA 8 34B irradiation position with thermal and epithermal average neutron fluxes of 4.7×10^{12} cm^{-2} s^{-1} and 7.4×10^{11} cm^{-2} s^{-1}, respectively. Irradiation times were 15 and 24 h for the thermal and resonance integral cross-section measurements, respectively.

The time interval between the end of the irradiation and the beginning of the residual radioactivity measurement was approximately 15 d for the Cd-covered irradiated bottle and 130 d in the case of bare irradiated samples.

TABLE I. Monitor activation parameters. F and G_{epi} were calculated as indicated in Ref. [8]. The numbers in parentheses are the standard deviations in units of the quantity's least significant digit. The quantities σ_0, I, and g were obtained from Ref. [9].

Flux monitor	σ_0	I	g	F	G_{epi}
^{197}Au	98.8(3) b	1560(40) b	1.01	0.9999(2)	0.99(2)

The thermal and epithermal average neutron fluxes were monitored through the ^{197}Au$(n,\gamma)^{198}$Au reaction using foils of Au-Al alloy containing 0.1% of gold in all the irradiations. These foils were irradiated in pairs with and without a 0.5-mm-thick Cd shield. The accuracy in the Au content in the alloy was previously checked by simultaneous irradiation with pure gold foils.

The thermal average neutron flux was obtained applying the Westcott formalism [7], which gives

$$\phi_{th} = \frac{(A_b - F_{\mathrm{Cd}}A_{\mathrm{Cd}})}{FN_0\sqrt{\frac{\pi T_0}{4T}}\sigma_0(g+rs')}\frac{R'}{(R'-1)}, \qquad (1)$$

where

A_b,A_{Cd} = saturated activities of bare and Cd covered monitor foils, respectively;

F_{Cd} = cadmium ratio correction factor;

$R'/(R'-1)$ = ratio between total and sub-cadmium neutron density;

F = correction due to thermal neutron absorption in the foil in the neutron field;

N_0 = number of atoms in the monitor foil;

T_0,T = absolute reference (20 °C) and moderator neutron temperatures;

σ_0 = monitor thermal cross section;

g = correction due to the departure from $1/v$ cross section behavior;

r = epithermal neutron fraction;

s' = Westcott factor between μkT and the Cadmium cut-off energy.

The epithermal average neutron flux was calculated using

$$\phi_{epi} = \frac{A_{\mathrm{Cd}}}{N_0 G_{epi} I}\ln\frac{E_2}{E_1}, \qquad (2)$$

where

G_{epi} = self-shielding factor for resonance neutrons;

I = Au resonance integral;

E_1,E_2 = lower and upper energy limits for the resonance integral (0.5 eV and 1 MeV).

Table I shows the activation parameters used for the average neutron fluxes determination.

D. Activity measurement

The gamma-ray measurements were performed with a HPGe detector (35% ORTEC), shielded by a 10-cm-thick lead wall, using live time counting methodology. The sources

TABLE II. Decay data used in the efficiency calibration and cross section measurements [6]. The numbers in parentheses are the standard deviations in units of the quantity's least significant digit.

Radionuclide	Half-life (d)	Gamma-ray energy (keV)	Photons per decay (%)
^{54}Mn	312.3(4)	834.843(6)	99.9758(24)
^{57}Co	271.70(9)	122.0614(3)	85.60(17)
		136.4743(5)	10.68(8)
^{58g}Co	70.82(3)	810.775(9)	95.57(47)
^{60}Co	1925.5(5)	1173.238(4)	99.857(22)
		1332.502(5)	99.983(6)
^{133}Ba	3862(15)	80.998(5)	34.11(28)
		276.398(1)	7.147(30)
		302.853(1)	18.30(6)
		356.017(2)	61.94(14)
		383.851(3)	8.905(29)
^{137}Cs	$1.102(6)\times10^4$	661.660(3)	85.1(2)
^{152}Eu	4933(11)	121.7824(4)	28.37(13)
		244.6989(10)	7.53(4)
		344.2811(19)	26.57(11)
		778.903(6)	12.97(6)
		964.055(4)	14.63(6)
		1408.022(4)	20.85(9)
^{198}Au	2.6943(8)	411.8044(11)	99.448(8)

were placed in holders on the detector axis in well defined arrangements: the near arrangement, with a 2-mm lead absorber and 10-mm distance between source and detector capsule, or the far arrangement, without absorber and 250-mm distance from source to detector capsule. The efficiency curve for sources in the far arrangement, fitted by the least-squares method [10,11], was calibrated with ^{152}Eu, ^{137}Cs, ^{133}Ba, ^{60}Co, ^{57}Co, and ^{54}Mn standard sources. The decay scheme data are shown in Table II [6,12]. Decay corrections were applied whenever required.

The ^{57}Co activities in the irradiation samples were found using a standard source inside a quartz bottle, similar to the irradiation samples, to take into account the absorption of the low-energy gamma rays. First, a source in collodium substract was prepared from a known aliquot of a ^{57}Co solution and calibrated in a $4\pi\beta$-γ coincidence system [13]. In sequence, another aliquot of the same solution, corresponding to 24.96(7) kBq as a result of the calibration, was dropped inside a quartz bottle. Finally, the gamma-ray spectra of the irradiated samples and the calibrated source were taken, and the ratio of the observed 122-keV γ-ray peak areas allowed the activities determination.

Special measurements were done to check that the atoms of ^{57}Co were located on the bottom of the quartz bottle. Also, the activity of each sample was measured before and after the irradiation to check that the material was kept in place during all the experimental procedure. No other correction besides the radioactive decay was required when comparing the ^{57}Co activities before and after irradiation.

The 810-keV γ rays from the irradiated samples were observed in the near arrangement to calculate the induced

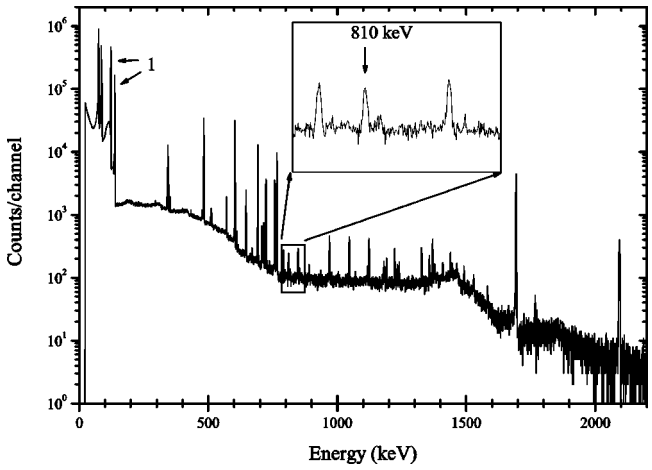

FIG. 2. Gamma spectrum of 20-h live time of the ^{57}Co sample after 15-h irradiation without cadmium cover and 129-d waiting time. The dispersion is 0.2 keV/channel.

^{58}Co activity. The required detection efficiency was obtained taking into account the source size, since the internal diameter of the quartz bottles was 7 mm. We used the fact that, in the far arrangement, the sample size had negligible effect in the efficiency. First, using the efficiency at 810 keV evaluated with the calibration curve in the far arrangement, we obtained the ^{58}Co samples contaminant activity before irradiation. Once these activity values had been determined, the measurement of the same samples in the near arrangement provided the efficiency.

III. EXPERIMENTAL RESULTS

A. ^{58}Co observation

Figures 2 and 3 show gamma spectra of the samples irradiated with and without cadmium cover. The 122- and 136-keV ^{57}Co γ rays are marked "1" in both figures, where the insets show the 810-keV ^{58}Co γ-ray peak standing out in relief. In spite of the pile-up rejection, the large activity of ^{57}Co in the measured spectra lead to the pile up of its more intense gamma rays with the gamma transitions following ^{56}Co decay. The worst pile-up interference corresponds to the sum between the 122-keV ^{57}Co γ-ray with the 692-keV ^{58}Co, which falls near the 810-keV peak. The insets of Figs. 2 and 3 show that the detector could resolve the peak of interest from the pile up peak.

The gamma spectrum of an empty quartz bottle irradiated without cadmium cover during 15 h and 21 d waiting time is shown in Fig. 4. The spectrum was obtained with a source to detector capsule distance equal to 250 mm without Pb absorber. The inset corresponds to the 810-keV energy region, showing that the observed ^{58}Co γ-ray peak is not mixed with peaks arising from activities in the irradiation bottle.

B. Contaminant analysis

We performed a detailed contaminants analysis using a quartz sample prepared as described in Sec. II B. We dropped an equal amount of the HCl solution used to dilute

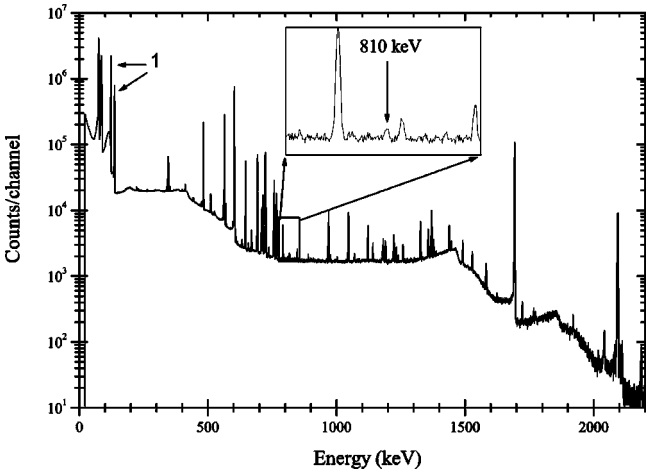

FIG. 3. Gamma spectrum of 60-h live time of the ^{57}Co sample after 24-h irradiation with cadmium cover and 16-d waiting time. The dispersion is 0.2 keV/channel.

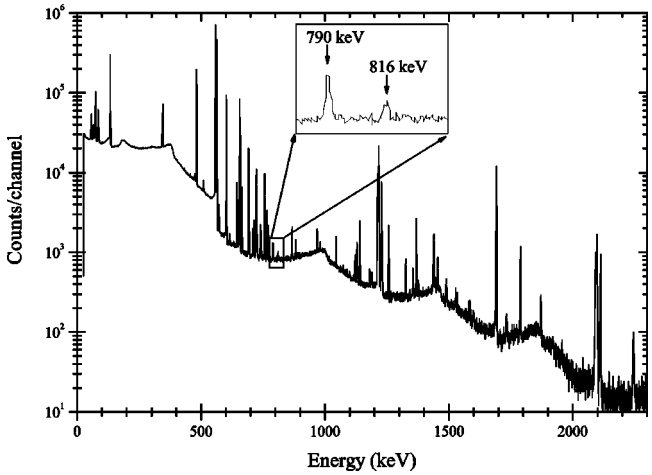

FIG. 4. Gamma spectrum of 80-h live time of a quartz sample after 15-h irradiation without cadmium cover and 21-d waiting time. The dispersion is 0.2 keV/channel.

the Amersham radioactive solution, waited until solution dryness, sealed the quartz bottle, and irradiated the sample for 15 h in the EIRA 8 34B irradiation position.

The sample was measured 21 days after the end of the irradiation. The detector system was calibrated in energy with standard sources of ^{152}Eu and ^{60}Co, as well as ^{40}K and ^{24}Na produced from K and Na present in the irradiation bottle. The full width at half maximum was calibrated with the most prominent observed singlet peaks and used to check the spectral purity of each observed line. In the 80-h background spectrum obtained, the gamma lines presented in the Ejnisman [14] work were identified. We also observed peaks at energies of 596 and 803 keV from gamma rays produced in the reactions ^{73}Ge$(n,n')^{73*}$Ge and ^{206}Pb$(n,n')^{206*}$Pb caused by background neutrons on the large masses of the germanium detector and the lead shielding [15], respectively.

After taking into account the background and pile-up effects, the remaining peaks were assigned to the following radioactive nuclides: ^{182}Ta, ^{124}Sb, ^{122}Sb, ^{95}Zr, ^{95}Nb, ^{175}Hf, ^{181}Hf, ^{76}As, ^{140}La, and ^{24}Na. They were identified by their half-lives and gamma ray spectra, comparing the emission probabilities of the suspected contaminants to the peak areas after efficiency correction.

C. Decay and burn-up calculations

Besides the radioactive decay, two other effects must be taken into account for a correct determination of ^{58}Co produced by neutrons in the irradiation. One correction comes from the existence of two isomeric states, whose formation ratio was evaluated theoretically because the low energy and intensity of the gamma rays following ^{58m}Co took its observation out of reach of our experimental method. The other correction is due, surprisingly, to the burn-up resulting from the very large neutron absorption cross sections of ^{58}Co and ^{58m}Co, respectively 1.88×10^{3} b and 1.36×10^{5} b [16].

Assuming that during the experimental measurements, many days after the end of the irradiation, all the 9 h ^{58m}Co formed had decayed to ^{58}Co, the physical quantity measured is approximately the sum of the cross sections of both isomers, σ_{m+g}, with a weak dependence on the isomer formation ratio. Calling the isomer formation ratio $\sigma_m/\sigma_g = x$, the number of ^{58}Co atoms at the end of the irradiation is given by

$$N_{58}^{t_i} = N_{58}^{0} e^{-(\lambda_{58}+\sigma_{58}\phi_{th})t_i} + N_{57}\sigma_{57}\phi_{th}\left\{\frac{(1-x)}{(\lambda_{58}+\sigma_{58}\phi_{th})}\left[1-e^{-(\lambda_{58}+\sigma_{58}\phi_{th})t_i}\right] + \frac{x\lambda_{58m}}{(\lambda_{58m}+\sigma_{58m}\phi_{th})}\left[\frac{(1-e^{-(\lambda_{58}+\sigma_{58}\phi_{th})t_i})}{(\lambda_{58}+\sigma_{58}\phi_{th})}\frac{e^{-(\lambda_{58m}+\sigma_{58m}\phi_{th})t_i}-e^{-(\lambda_{58}+\sigma_{58}\phi_{th})t_i}}{[\lambda_{58}-\lambda_{58m}+\phi_{th}(\sigma_{58}-\sigma_{58m})]}\right]\right\}, \quad (3)$$

where

$N_{58}^{t_i}$= number of ^{58}Co atoms at the end of the irradiation;

N_{58}^{0}= number of ^{58}Co atoms (the sample contaminant) at the beginning of the irradiation;

λ_r= decay constants of ^{58}Co and ^{58m}Co;

σ_r=^{58}Co and ^{58m}Co activation cross sections;

ϕ_{th}= thermal average neutron flux obtained by applying the expression (1);

t_i= irradiation time.

The isomer formation ratios x, calculated by applying the Huizenga and Vandenbosch formalism [17] for the most likely gamma ray cascade multiplicities and compound state

TABLE III. Calculated isomer ^{58m}Co to ground state ^{58}Co formation ratio x according the gamma-ray cascade multiplicity M_γ and the compound state spin J [17].

M_γ	$J=3$	$J=4$
3	0.28	0.57
4	0.32	0.51

spins, are presented in Table III. These ratios can be compared with the experimental value for the ^{60}Co isomers produced in the ^{59}Co$(n,\gamma)^{60}$Co reaction, $x=0.55$ [9], due to the similarity between ^{57,58}Co and ^{59,60}Co structures; in particular, the spins of the targets are the same, as well as the products' m and g spins.

D. Cross section and resonance integral determination

The expressions for the thermal cross section σ_{th} and resonance integral I are

$$\sigma_{th} = \frac{A_{58}\lambda_{57}}{A_{57}\phi_{th}\sqrt{\frac{4T}{\pi T_0}}}, \tag{4}$$

$$I = \frac{A_{58c/Cd}\lambda_{57}}{A_{57c/Cd}\phi_{epi}}\ln\frac{E_2}{E_1}, \tag{5}$$

where

A_{57},$A_{57c/Cd}$ =^{57}Co activities in the targets without and with the cadmium cover, respectively;

A_{58},$A_{58c/Cd}$ = ^{58}Co reaction product activities at the end of irradiation without and with the cadmium cover, respectively;

ϕ_{th},ϕ_{epi} = thermal and epithermal average neutron fluxes, respectively, determined with the Au-Al monitors;

T,T_0 = moderator and reference temperatures, 44 and 20 °C, respectively;

E_1,E_2 = neutron spectrum integration limits, 0.5 eV and 1 MeV, respectively;

λ_{57} = ^{57}Co decay constant.

Two irradiations were performed for the resonance integral measurement and other two for the thermal cross section measurement. The values obtained by formulas (3)–(5) with the different isomer formation ratio values x from Table III are not much different, hence the final results are their average and the corresponding dispersion is added in quadrature to the other uncertainties. Table IV shows the thermal and resonance integral cross sections.

TABLE IV. Thermal and resonance integral ^{57}Co$(n,\gamma)^{58}$Co reaction cross sections. The values correspond to the ^{58m}Co plus ^{58g}Co cross sections. The numbers in parentheses are standard deviations in units of the least significant figure.

Thermal	Resonance integral
51(5) b	20.0(19) b

IV. CROSS-SECTION ENERGY DEPENDENCE

A. Single resonant capture

The determination of the neutron cross-section energy dependence through some type of theoretical calculation requires more experimental information than that provided by the measured thermal and resonance integral cross sections. For very light nuclei, the energies of the first resonances can be obtained considering the level sequence at neutron binding energies, allowing a good description of the neutron cross section above a few hundred keV of kinetic energy [18,19]. In the case of ^{57}Co, the level density is already too high at the energy of the compound nucleus (B_n =8.573 MeV) for such approach. Therefore we intend to describe the cross section by a combination of two models: at low energies, from thermal to a few keV, we used the resonance capture model and, for higher energies, a statistical model. The boundary of the energy region where we change from one model to the other was called edge energy, E_{edge}.

The total cross section of a neutron with kinetic energy E, σ_T, has two components, the elastic σ_{el}, and the capture σ_{CN} cross sections:

$$\sigma_T = \sigma_{el} + \sigma_{CN}. \tag{6}$$

For energies around the first resonance, we can describe the cross section via the Breit-Wigner resonant capture formula. Then, the components are given by

$$\sigma_{el} = \frac{\pi}{k^2}g(I,J)\frac{(\Gamma_n)^2}{(E-E_0)^2+\frac{\Gamma^2}{4}},$$

$$\sigma_{CN} = \frac{\pi}{k^2}g(I,J)\frac{\Gamma_n\Gamma_\gamma}{(E-E_0)^2+\frac{\Gamma^2}{4}} \tag{7}$$

which are functions of the partial widths of neutron and gamma emission, Γ_n and Γ_γ, respectively, the total width Γ =Γ_γ+Γ_n, the resonance energy E_0, the wave number k, and

$$g(I,J) = \frac{2J+1}{(2I+1)(2s+1)},$$

where I and J are the angular momenta of target and compound nuclei, respectively, and s is the neutron spin.

The partial neutron width was calculated by

$$\Gamma_n = \frac{\langle D\rangle}{2\pi}\sum_l T_l, \tag{8}$$

where $\langle D\rangle$ is the evaluated average level spacing at the neutron binding energy [20], and T_l are the partial transmission coefficients for different values of the orbital angular momentum. If we assume that only the S wave gives an important contribution, this equation reduces to

$$\Gamma_n = \frac{\langle D\rangle}{2\pi}T_0. \tag{9}$$

The transmission coefficient was calculated via optical model, with nuclear potential parameters from Wilmore and Hogdson [21].

The partial width of γ emission was calculated with the Mughabghab's formulation [22], where Γ_γ is a function of the neutron binding energy B_n and the average angular momenta of neutrons and protons near the Fermi level, $\langle J_n \rangle$ and $\langle J_p \rangle$, respectively,

$$\Gamma_\gamma = \Gamma_\gamma(B_n, \langle J_n \rangle, \langle J_p \rangle), \tag{10}$$

being energy independent. Both averaged angular momentum were calculated using the Barrier code [23].

For energies well above the first resonance the statistical model was used. The neutron absorption cross section is described by

$$\sigma_{STAT}(E) = \frac{\Gamma_\gamma(E)}{\Gamma_n(E) + \Gamma_\gamma(E)} \sigma_R, \tag{11}$$

where σ_R is the reaction cross section obtained from the optical model.

The thermal cross section is calculated by the value of σ_{CN} at $E = 0.025$ eV and the resonance integral by

$$I = \int_{0.5\ \mathrm{eV}}^{E_{edge}} \frac{\sigma_{CN}(E)}{E} dE + \int_{E_{edge}}^{1.0\ \mathrm{MeV}} \frac{\sigma_{CN}(E)}{E} dE, \tag{12}$$

where E_{edge} separates the resonance and statistical models applicability regions. It should be noticed that the thermal and resonance integrals are not independent quantities since it is the first resonance that gives the main contribution to the resonance integral.

B. Single-resonance calculations for ^{59}Co and ^{57}Co

This formalism is very successful in the case of ^{59}Co, a very well studied nucleus with structure similar to ^{57}Co. The position and width of the first resonance are well determined [24] and both the thermal cross section and resonance integral are reproduced using a single resonance. It may be worth to point out that about 80% of the resonance integral comes from the first term of Eq. (12), which gives the contibution of the neutrons below the edge energy, taken as 1 keV.

In order to establish the parameters of the Breit-Wigner resonance in the case of ^{57}Co, the resonance energy that gives the experimental thermal neutron capture cross section value for a given neutron resonance width Γ_n is plotted in Fig. 5, for the two possible angular momenta of this isolated resonance assuming a *S*-wave neutron, $J^\pi = 3^-$ and $J^\pi = 4^-$, and one of the possible angular momenta assuming a *P*-wave neutron, $J^\pi = 2^+$.

Figure 6 shows the calculated resonance integral, Eq. (12), as a function of the resonance energy, choosing a different neutron width for each resonance energy value to fit the experimental thermal neutron cross section (Fig. 5). It can be seen that the calculated integral resonance always overestimates the experimental value. Therefore we conclude that only one isolated resonance cannot describe the experimental results. It is important to note that the first term of Eq. (12) alone already overestimates the experimental resonance integral whatever the resonance energy and neutron width that fit the experimental thermal cross section.

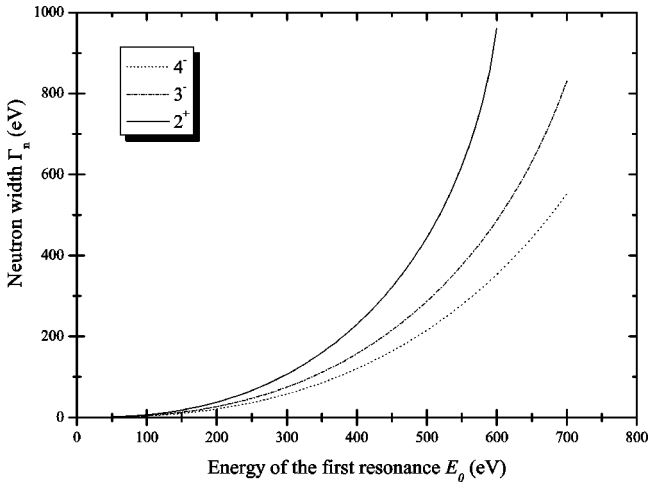

FIG. 5. Plot of the resonance parameters, neutron width and resonance energy, that give the ^{57}Co experimental thermal neutron cross section, for the two possible angular momenta of this isolated resonance assuming a *S*-wave neutron, $J^\pi = 3^-$ and $J^\pi = 4^-$, and one of the possible angular momenta assuming a *P*-wave neutron, $J^\pi = 2^+$.

Although ^{59}Co and ^{57}Co have similar thermal neutron absorption cross sections, 37 and 51 b, respectively, the ^{59}Co resonance integral, $I_0 \sim 70$ b, is much greater than the same quantity for ^{57}Co, $I_0 \sim 20$ b. Therefore we were led to consider two neighboring resonances at low energy in order to obtain the correct magnitude of the resonance integral, because it can be reduced due to the interference between the two resonances. A different formalism is required for the multilevel resonant capture, as described below.

C. Reich-Moore formulation for multilevel resonant capture

The effects of destructive interference between the resonances in the Reich and Moore formalism [25], when de-

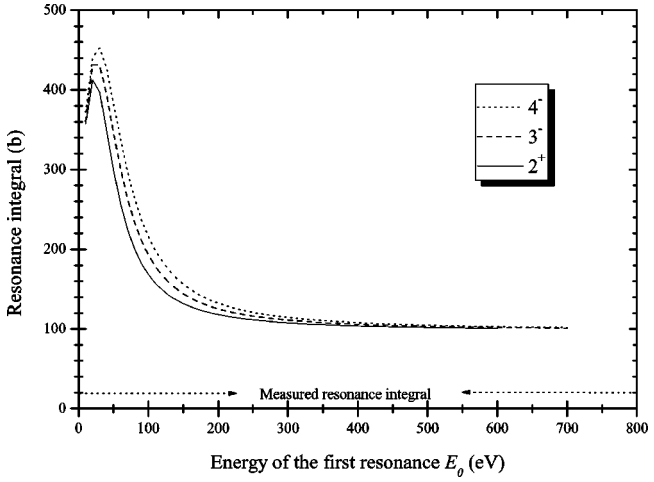

FIG. 6. Calculated integral resonance in function of the position of the first isolated resonance for ^{57}Co. The neutron width changes with the resonance energy as plotted in Fig. 5.

scribing the multilevel resonant capture, was successfully applied in previous studies on nonfissile nuclei [26,27]. We adopted this formalism to describe the ^{57}Co(n,γ) cross-section as

$$\sigma_{n,\gamma} = \frac{4\pi}{k^2} g(I,J)[\mathrm{Re}(\rho_{nn}) - |\rho_{nn}|^2], \tag{13}$$

where

$$\rho_{nn} = 1 - [(I-K)^{-1}]_{nn} \tag{14}$$

and

$$[(I-K)]_{nn} = 1 - \frac{i}{2}\sum_r \left[\frac{\Gamma_{nr}}{E_r - E - i\frac{\Gamma_r}{2}}\right]. \tag{15}$$

Here the sum is done over the resonances r with energy E_r and neutron and gamma widths Γ_{nr} and Γ_r, respectively.

Although one resonance is not enough to fit the available data, two resonances provide more free parameters than required to fit the thermal and resonance integral cross sections. To help to find the suitable values, we rewrote the formulas in function of the distance between the two first resonances, ΔE, and the energy of the first resonance, E_0. We obtained

$$\rho(E_0,\Delta E,E) = 1 - \left[1 - \frac{i}{2}\left(\frac{\Gamma_{n1}}{E_0 - E - i\frac{\Gamma_1}{2}} + \frac{\Gamma_{n2}}{E_0 + \Delta E - E - i\frac{\Gamma_2}{2}}\right)\right]^{-1}, \tag{16}$$

and the capture cross section:

$$\sigma_{n,\gamma}(E_0,\Delta E,E) = \frac{4\pi}{k^2} g(I,J)[\mathrm{Re}(\rho(E_0,\Delta E,E)) - |\rho_{nn}(E_0,\Delta E,E)|^2]. \tag{17}$$

That means that we have four variables E_0, Γ_{n1}, Γ_{n2}, and ΔE, with only two conditions: the thermal and the resonance integral experimental cross section values. Consequently, there will be a family of possible cross section curves.

The resonance integral was calculated in function of the first resonance energy for different values of the distance between the first and second resonances, assuming that the widths of both resonances are equal and chosen to fit the thermal cross section. The results are plotted in Fig. 7, where it can be seen that in a broad range of values around $E_0 \sim 600$ eV the calculated values are compatible with the measured cross section, taking into account the experimental uncertainties. Note that the single criterion adopted to choose the resonance parameter values was that they were positive numbers. Table V shows a few sets of model parameters, considering different first resonance energies, which fit the measured thermal (n,γ) cross section and give the resonance integral value within experimental error bar.

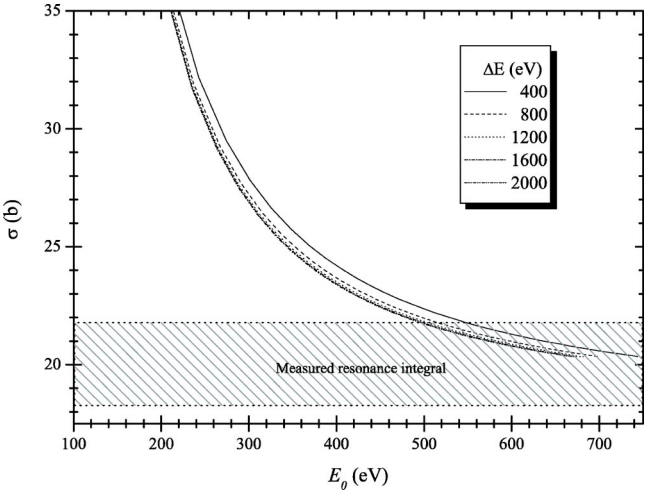

FIG. 7. Calculated ^{57}Co resonance integral in function of the first isolated resonance position for some energy separations between the two first resonances. The neutron width for both resonances are equal and were chosen to fit the thermal cross section.

The ^{57}Co calculated (n,γ) cross section curve in function of the neutron energy using the model described here and some of the resonance parameters listed in Table V are shown in Fig. 8, assuming $J^\pi = 3^-$ for both resonances.

D. Maxwellian averaged ^{57}Co$(n,\gamma)^{58}$Co cross section

For astrophysical model calculations, the Maxwellian averaged cross section is needed. Bao [26] evaluated the Maxwellian averaged cross sections (MACS) in the range between $kT = 5$ and 100 keV for many radioactive nuclides.

We obtained the Maxwellian averaged cross section for ^{59}Co and ^{57}Co as

$$\langle\sigma\rangle_{kT} = \frac{2}{\sqrt{\pi}}\frac{1}{(kT)^2}\int_0^\infty \sigma(E) E \exp\left(-\frac{E}{kT}\right) dE. \tag{18}$$

This average is sensitive to the cross section $\sigma(E)$ energy dependence.

Using the results obtained in previous sections for the capture cross section we divided Eq. (18) in two terms:

TABLE V. Parameters of the Reich-Moore resonance capture with two resonances fitting the measured thermal (n,γ) cross section and where the resonance integral equals 21 b. The angular momentum J^π was adopted as 3^- in all the cases, as well as the gamma width $\Gamma_\gamma = 0.391$ eV and $\Gamma_n = 560$ eV.

E_0 eV	ΔE eV
546	400
609	800
596	1200
590	1600
587	2000

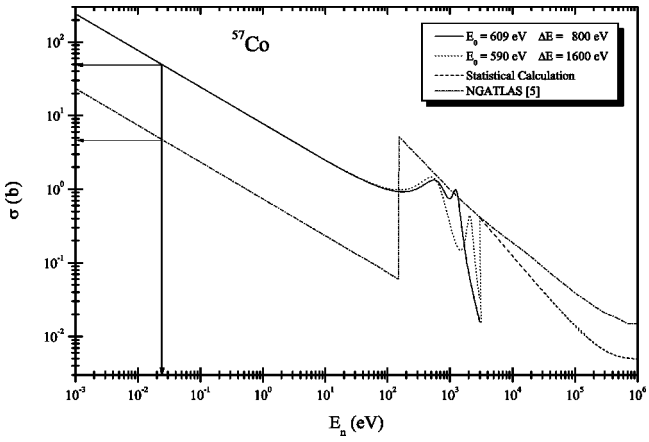

FIG. 8. Calculated (n,γ) cross section in function of the neutron energy within the model described here with two resonances and Γ_n=560 eV. Our results are compared with the previous Kopecky [5] evaluation. The thermal cross section for both curves is indicated.

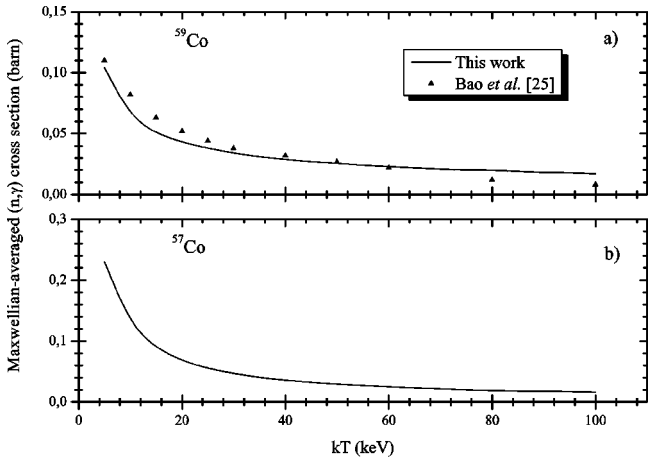

FIG. 9. Maxwellian averaged cross sections using the model developed in this work. (a) shows the results for ^{59}Co compared with Ref. [26] and (b) for ^{57}Co.

$$\langle\sigma\rangle_{kT} = \frac{2}{\sqrt{\pi}}\frac{1}{(kT)^2}\int_0^{E_{edge}} \sigma_{CN}(E)E\exp\left(-\frac{E}{kT}\right)dE + \frac{2}{\sqrt{\pi}}\frac{1}{(kT)^2}\int_{E_{edge}}^{\infty} \sigma_{STAT}(E)E\exp\left(-\frac{E}{kT}\right)dE. \quad (19)$$

The first one is related to the resonant capture and the second, to the statistical process. The value of E_{edge} was adopted as $E_0+10\Gamma_n$ for ^{59}Co.

Figure 9(a) shows our MACS results for ^{59}Co using the model developed in this work, which are very similar to Bao's [26] results, and Fig. 9(b) shows the results for ^{57}Co evaluated with the cross sections shown in Fig. 8 and $E_{edge}=E_0+\Delta E+\Gamma_n$. The MACS temperature dependence for both nuclei are similar, with the absolute value for a given temperature being smaller for ^{57}Co. This behavior is due to differences in statistical parameters and neutron binding energy; the differences in the cross sections in the first few keV did not show up in the calculated averages.

V. DISCUSSION AND CONCLUSION

The thermal neutron cross section for the ^{57}Co$(n,\gamma)^{58}$Co reaction obtained in the present work was 51(5) b. The obtained value differs considerably from that encountered in existing databases ~6 b for ~0.025 eV neutrons obtained from the Kopecky evaluation [5]. The resonance integral obtained was 20.0(19) b. The uncertainty in this result was due to the presence of ^{58}Co in the solution used to prepare the target and the low induced residual activity by the resonant capture reaction in the small target mass.

It was proven that a single resonance below about 1 keV incident neutron energy properly positioned to give the observed value of the thermal cross section cannot account for the observed resonance integral. Therefore the energy dependence of the neutron absorption cross section was calculated considering two isolated resonances at energies about 1 keV and the statistical model for higher energies. Although it is not possible to be sure that there is not a third resonance about 1 keV, this is the simplest model that can reproduce both the observed thermal and resonance integral cross sections. Considering the ^{58}Co level density near the binding energy, finding three levels in a region about 1 keV wide is more unlikely than the already unlikely event of finding two as assumed.

Using the model described here, the Maxwellian averaged ^{57}Co neutron absorption cross section was evaluated in the 5–100-keV neutron temperature range.

ACKNOWLEDGMENTS

The authors would like to thank the IEA-R1 reactor staff for helping in the irradiations. We are also grateful to the CNPq (Conselho Nacional de Pesquisas, Brazil) and FAPESP (Fundação de Amparo à Pesquisa do Estado de São Paulo, Brazil) for partial support of this research.

[1] N. Maidana, V. R. Vanin, P. R. Pascholati, M. S. Dias, and M. F. Koskinas, J. Nucl. Sci. Technol. **2**, 441 (2002).

[2] J. D. Kurfess, W. N. Johnson, R. L. Kinzer, R. A. Kroeger, M. S. Strickman, J. E. Grove, M. D. Leising, D. D. Clayton, D. A. Grabelsky, W. R. Purcell, M. P. Ulmer, R. A. Cameron, and G. V. Jung, Astrophys. J. Lett. **399**, L137 (1992).

[3] N. Maidana, M. S. Dias, and M. F. Koskinas, Radiochim. Acta **83**, 117 (1998).

[4] N. Maidana, M. S. Dias, and M. F. Koskinas, Radiochim. Acta **89**, 1 (2001).
[5] J. Kopecky, *Atlas of Neutron Capture Cross Section*, INDC(NDS)-362 (IAEA, Vienna, 1997).
[6] R. B. Firestone, *Table of Isotopes*, 8th ed. (Wiley, New York, 1996).
[7] C. H. Westcott, *Effective Cross Section Values for Well-Moderated Thermal Reactor Spectra*, 3rd ed. (Atomic Energy of Canada, Chalk River, 1960).
[8] *Neutron Fluence Measurements*, Technical Report Series 107 (IAEA, Vienna 1970).
[9] J. H. Baard, W. L. Zijp, and H. J. Nolthenius, *Nuclear Data Guide for Reactor Neutron Metrology* (Kluwer Academic, Dordrecht, 1989).
[10] R. M. Castro, V. R. Vanin, O. A. M. Helene, P. R. Pascholati, N. L. Maidana, M. F. Koskinas, and M. S. Dias, J. Nucl. Sci. Technol. **2**, 485 (2002).
[11] R. Tramontano and V. R. Vanin, Appl. Radiat. Isot. **51**, 323 (1999).
[12] *X-Ray and Gamma-Ray Standards for Detector Calibration*, Report IAEA-TECDOC-619 (IAEA, Vienna 1991).
[13] G. Ratel and C. Michotte, Metrologia **40**, 06004 (Technical Supplement) (2003).
[14] R. Ejnisman and P. R. Pascholati, Revista de Física Aplicada e Instrumentação, **9(4)**, 139 (1994).
[15] *American National Standard for Calibration and Use of Germanium Spectrometers for the Measurement of Gamma-Ray Emission Rates of Radionuclides* ANSI N42.14-1999 (American National Standard Institute, New York, 1999).
[16] W. Seelmann-Eggebert, G. Pfennig, H. Münzel, and H. Klewe-Nebenius, *Nuklidkarte*, 5th ed. (Institut für Radiochemie Kernforschungszentrum, Kalsruhe GmbH, 1981).
[17] J. R. Huizenga and R. Vandenbosch, Phys. Rev. **120**, 1305 (1960).
[18] J. Meissner, H. Schatz, H. Herndl, M. Wiescher, H. Beer, and F. Kappeler, Phys. Rev. C **53**, 977 (1996).
[19] J. Meissner, H. Schatz, J. Gorres, H. Herndl, M. Wiescher, H. Beer, and F. Kappeler, Phys. Rev. C **53**, 459 (1996).
[20] A. Bohr and B. Mottelson, *Nuclear Structure: Single-Particle Motion* (Benjamin, New York, 1975), Vol. I.
[21] D. Wilmore and P. E. Hodgson, Nucl. Phys. **55**, 673 (1964).
[22] S. F. Mughabghab, M. Divadeenam, and N. E. Holden, *Neutron Cross Sections* (Academic, New York 1981), Vol. I, part A.
[23] F. Garcia, O. Rodriguez, J. Mesa, J. D. T. Arruda-Neto, V. P. Likhachev, E. Garrote, R. Capote, and F. Guzmán, Comput. Phys. Commun. **120**, 57 (1999).
[24] P. F. Rose, ENDF-201 ENDF/B-VI Summary Documentation, Report No. BNL-NCS-17541-201, Associated Universities, INC., Brookhaven National Laboratory, Upton, NY, 1991.
[25] C. W. Reich and M. S. Moore, Phys. Rev. **111**, 929 (1958).
[26] Z. Y. Bao, H. Beer, F. Kappeler, F. Voss, K. Wisshak, and T. Rauscher, At. Data Nucl. Data Tables **76**, 70 (2000).
[27] K. Devan and K. S. Keshavamurthy, Ann. Nucl. Energy **26**, 1253 (1999).